Acta Manilana 70 (2022), 29-46

ISSN: 0065-1370

Acta Manilana

journal homepage: https://actamanilana.ust.edu.ph/

Polyaniline/agricultural waste microcellulose composites as electrode materials for supercapacitors

Felicidad Christina Ramirez-Peñafiel[1,2]*, Riezel E. de Guzman[1], Albert Solomon K. Perez[1,3], and Christina A. Binag[1,2,3]

[1]Department of Chemistry, College of Science, University of Santo Tomas, España Boulevard, 1015 Manila
[2]Research Center for the Natural and Applied Sciences, University of Santo Tomas, España Boulevard, 1015 Manila
[3]The Graduate School, University of Santo Tomas, España Boulevard, 1015 Manila

Graphical Abstract

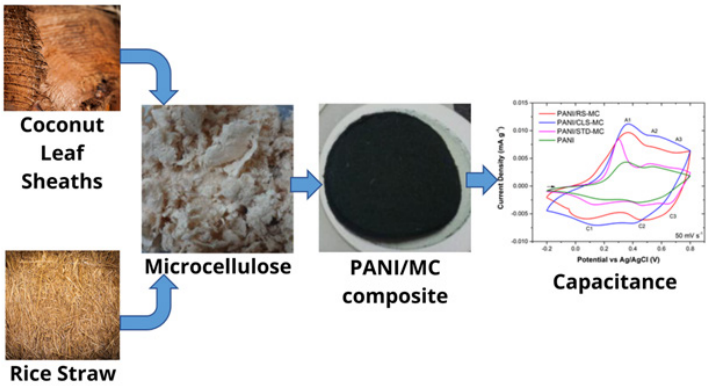

Abstract

Supercapacitors are energy storage devices that employ carbon, metal oxides, and conducting polymers as electrode materials. Polyaniline (PANI) was polymerized onto microcellulose (MC) to produce an electroactive material suitable for supercapacitor electrode applications. Microcellulose was prepared from cellulose extracted from *Cocos nucifera* L. (coconut, CLS) leaf sheaths and *Oryza sativa* straw (rice, RS). Delignification and bleaching procedures yielded 45% and 28% cellulose from CLS and RS, respectively, followed by acid hydrolysis to produce MC. Acid hydrolysis of the extracted cellulose produced MC. PANI was chemically polymerized onto MC using a 50:50, 70:30, and 90:10 aniline:MC ratios. PANI/MC composites were then characterized by SEM, TGA, FTIR, four-point probe conductivity testing and cyclic voltammetry. SEM micrographs indicated the composite was composed of thin ribbon-like strands with a rough surface coating. TGA revealed that extracted cellulose (CLS – 312.55 °C; RS - 331.50 °C) had lower purity compared to standard cellulose (335.28 °C). FTIR spectra of the composites showed characteristic peaks of both pure PANI and MC. PANI/MC composites with 90:10 ratio gave the highest conductivity values, ranging from 36.4 μScm^{-1} to 39.0 μScm^{-1}; and specific capacitance values of 51.2 F g^{-1} to 109 F g^{-1} at 50 mV s^{-1}. The results showed effective utilization of waste residues capable of increasing the potential of PANI as an electrode material for supercapacitors.

Keywords: polyaniline, coconut leaf sheaths, rice straw, microcellulose, supercapacitor electrodes

Corresponding author: frramirez@ust.edu.ph
DOI: https://doi.org/10.53603/actamanil.70.2022.mgcy2771

Introduction

Society's demand for power has greatly increased due to new technological innovations [1]. This large power requirement, together with the decreasing availability of fossil fuels and climate change, has driven society to shift from fossil fuels to renewable sources of energy [2–5]. However, many renewable sources of energy, such as solar and wind power, are intermittent in nature and its irregular availability prevents it from becoming the primary source of power in many areas. This problem can be overcome by the development of new energy storage devices that can allow us to store and use this energy on demand [6,7]. To meet current technological demands, these devices must be able to store large amounts of energy, guarantee operational safety, be low cost, sustainable and maintain small size and weight for them to find applications in areas like mobile devices and transportation.

Supercapacitors store energy by separating charge on the surface of its electrode material. There are two types of supercapacitors – electric double-layer capacitors (EDLC) and pseudocapacitors. The distinction is based on the mechanism it separates charges. EDLCs electrostatically separate charge at the surface of the electrode material and electrolyte. Meanwhile pseudocapacitors, separate charge through redox or Faradaic reactions that occur at the surface of the electrode. High surface area carbon compounds are commonly used in EDLCs while conducting polymers and metal oxides are used in pseudocapacitors [4,8]. Supercapacitors can be charged-discharged many times without losing its energy storage capability (1,000,000 cycles) [1]. Its charge-discharge cycles occur very quickly (in less than a minute) leading to high power densities (1,000-10,000 W kg^{-1}) however, its energy density is quite low (~5 Wh kg^{-1}) [1,6,9].

To meet the energy requirements needed, the performance of supercapacitors need to be improved by developing new materials for its components – electrodes, electrolytes and separator materials. Among the three components, supercapacitor performance is highly dependent on the electrode material used [1,2,4]. This study would like to focus on the use a conducting polymer, polyaniline (PANI), coated onto microcellulose for supercapacitor applications.

Polyaniline is a conducting polymer with good electrical and redox properties, low cost, ease of synthesis and low environmental impact [10]. PANI is an excellent electroactive material, as it has a high theoretical capacitance of 3000 F g^{-1} [11]. PANI's capacitance can be modified by changing various factors during preparation, such as the synthetic route used, the thickness of the electrode, polymer morphology, and polymerization time [12]. PANI can be modified through different techniques to target desired capacitance values. These characteristics make PANI an ideal supercapacitor electrode material, however, one major drawback is that PANI has a poor charging and discharging cycle life. PANI, as an electrode material, shrinks and swells during charge and discharge cycles, which causes great mechanical stress to the material and causes the degradation of PANI [13]. To overcome PANI's poor mechanical strength and lessen degradation, numerous studies have combined PANI and a support material with good mechanical properties [14]. PANI has been combined with carbon nanotubes [15–19], metal-organic frameworks [20] nanocellulose/cellulose [14,21–27], and textiles [28–31].

Among the available support materials of the PANI composites, cellulose is the most abundant and renewable polymer [32,33]. Cellulose is a linear chain of beta-D-glucose residues found in the primary and secondary cell wall layer. Cellulose is notable for its high tensile strength because of its diverse –OH groups available for H-bonding. For this reason, wooden materials have remarkable durability. A cellulose molecule contains about 5,000 to 15,000 glucose residues while a cellulose fibril comprises about 500,000 cellulose molecules [34,35]. Cellulose fibrils' high tensile strength comes from the network of stacking intra- and inter- molecular H-bonding [35].

The Philippines, with 41.7% of its 30 million hectares of land dedicated to agriculture [36], can generate substantial amounts of biomass including agricultural residues [37]. Rice, coconuts, corn, sugarcane, bananas, pineapples, and mangoes are the most abundant crops planted with a total area of about 9 million hectares [38]. The Philippines is one of the top producers of *Cocos nucifera* L. coconut trees in the world. The coconut leaf sheath, found at the base of the leaf stalk is often burnt by farmers or is turned into handicraft. Rice plant (*Oryza sativa*) is also one of the major agricultural crops of the Philippines and its milling process generates massive amount of rice straws and husks (11.3 million tons per year) as waste products which are commonly disposed through open burning [39]. However, these waste products are lignocellulosic biomasses and contain substantial amounts of cellulose. Utilization of this biomass cellulose for various energy storage applications has caught the attention of several research groups, as it adds value to the waste material, reduces environmental pollution, and promotes the conservation of resources [40].

This study aims to chemically polymerize PANI onto microcellulose extracted from coconut leaf sheaths and rice straw, and to characterize these materials as supercapacitor electrode materials using SEM, FTIR, TGA, four-point probe technique and cyclic voltammetry.

Materials and methods

Materials. All reagents were of analytical grade. Ashless cellulose powder (Fisher) was used as standard (STD) cellulose. Aniline (ANI) (Sigma-Aldrich) monomer was distilled using a simple distillation setup to remove impurities. Distilled ANI was stored at 4^{o}C until use.

Plant sample collection and preparation. *Cocos nucifera* L. leaf sheaths (CLS) were collected from a coconut plantation field situated in Brgy. Sta. Clara, Sto. Tomas, Batangas, Philippines in September 2013 while *Oryza sativa* rice stralk (RS) was collected from Rizal, Nueva Ecija. Both plants were authenticated by the UST Herbarium.

The plant samples were cut into pieces, washed to remove mud and dirt, then dried in an oven (Binder) set at 80 ^{o}C for 48 h. The dried samples were ground in a Wiley mill grinder using a fine mesh (0.5 mm).

Cellulose extraction. Various methods (Table 1) were used to extract cellulose from the plant samples. Ground plant sample (~10 g) was subjected to dewaxing, delignification, bleaching, and purification to obtain cellulose.

Dewaxing was done by Soxhlet extraction using hexane (85 mL) followed by ethanol (85 mL) for 3 h each [41]. For delignification, the ground sample was soaked in 5% NaOH (Uni-Chem) for 12 h at 30 °C. The delignified sample was then filtered off the reaction mixture [41–45]. The dried sample was then bleached using 2% H_2O_2¬ (Sigma-Aldrich) in 4% KOH (J.T. Baker) (pH 11.8) for 8 h at 50 °C with a sample to solution ratio of 1 g : 25 mL. Lastly, in the purification step, the sample was immediately immersed in 250 mL 6.64 x 10^{-3} M acetic acid (Mallinckrodt) (pH 3-4) for 5 h at 70 °C [41]. The sample was oven-dried to obtain cellulose.

Table 1. Methods used to extract cellulose from plant samples

Steps	CLR		RS	
	M1	M2	T1	T3
Dewaxing	✓		✓	
Delignification		✓	✓	✓
Bleaching	✓	✓	✓	✓
Purification	✓	✓	✓	✓

Microcellulose Production. Extracted cellulose was subjected to acid hydrolysis, using 17.5 mL of 64 % H_2SO_4 (Mallinckrodt) for every gram of cellulose, to produce MC. The acid hydrolysis was performed for 60 minutes with stirring at room temperature. The hydrolysis was discontinued by adding the mixture to 10-fold of cold water. To remove excess acid, the colloid was subjected to dialysis (Carolina dialysis tubing) against distilled water until a neutral pH was obtained.

Preparation of Polyaniline/Microcellulose composite. PANI/MC composites were prepared using with 50:50, 70:30, and 90:10 PANI:MC ratios with 1 M HCl (J.T. Baker) as the dopant. The amount of the MC was made constant with varying amounts of ANI monomer and diluted to 100 mL using 1 M HCl. The resulting suspension was then sonicated (Branson2000) for 15 minutes. The MC-ANI suspension was incubated for 1 h at room temperature. After incubation, $(NH_4)_2S_2O_8$ (APS, Sigma-Aldrich) solution (in 100 mL 1 M HCl) with an APS to ANI ratio = 1.5 wt/wt, was then added to the MC-ANI dispersion. The polymerization mixture was stirred for 24 h at room temperature at 200 rpm (IKA KS-260) and was vacuum filtered using a Whatman cellulose nitrate membrane (0.45 μM) filter and then air dried to obtain the PANI/MC composite. Pure PANI was prepared using the same method excluding the MC.

Preparation of PANI/MC electrode. The electrode was prepared by mixing 10 mg of polyvinylidene fluoride (PVDF) in 800 μL N-methyl-pyrrolidine for 3 h. Around 80 mg of the prepared composite was ground with 10 mg of carbon black support material and was mixed with the PVDF/NMP solution and stirred for another 3 hours. A 10 μL portion of this slurry was spread by doctor blade method on the 1 cm x 1 cm surface of a titanium strip.

Characterization. Sample surface morphologies were analyzed using a Hitachi TM SEM at 15 KeV. The thermal stability of cellulose and PANI/MC were analyzed using a Perkin Elmer Thermogravimetric Analyzer (TGA) 4000 at a heating rate of 10 °C min-1 from 30 °C to 750 °C under N_2 gas atmosphere. A Shimadzu IR-Prestige21 was used to obtain the FTIR spectra of the extracted cellulose and composites using the KBr pellet method.

The electrical conductivities (σ) of the composites were measured at room temperature using a fabricated four-point probe method. Conductivity was calculated based on equation (1):

$$\sigma = \frac{\ln 2\, I}{\pi V t} \quad (1)$$

where σ is the calculated conductivity of the composite (μS cm^{-1}), I is the current measured (μA), V is the potential applied (V), and t is the film thickness (cm) of the composite.

Specific capacitance measurements were obtained via three-electrode cyclic voltammetry using an eDAQ potentiostat and Echem logger with an Ag/AgCl reference and platinum counter electrode; and the composite as working electrode for 10 scans at 50 mV s^{-1} with a potential window of – 0.2 V to + 0.8 V in a 1 M H_2SO_4 electrolyte solution. Specific capacitance (C_m) was calculated using equation (2):

$$C_m = \frac{1000}{2m\nu\Delta V} \int idV \quad (2)$$

where C_m is specific capacitance (F g^{-1}), m is the mass of electroactive material (g), ν is the scan rate (mV s^{-1}), v is the potential window (V), and idV is the area under the CV curve (AV).

Results and Discussion

Cellulose extraction and characterization. Coconut leaf sheaths and rice straw are mainly composed of cellulose, hemicellulose, lignin, and ash [46,47]. The amount of each component varies greatly in literature as shown in Table 2.

Table 2. Composition of CLS, RS, and cellulose recovered (wt%).

Component	CLS (%)[46]	RS (%)[47]
Cellulose	37 – 43	28 – 35.3
Hemicellulose	24 - 28	21.5 – 55
Lignin	26 – 28	11 – 24.4
Others / Ash	± 7	6 - 15
Cellulose Recovery (this study)	45.8	31.11

The first stage in cellulose extraction was the dewaxing step and it was done to remove extractives (waxes, oils, pectin, etc.) in the ground plant sample [8,48]. After Soxhlet extraction, the colorless solutions of hexane and ethanol turned turbid and yellow. This gave the implication that extractives such as oils and other organic compounds were initially present in the sample and were successfully removed. Visual inspection of the raw fibers and Soxhlet extracted fibers showed no significant change in the fibrous structure but signs of discoloration from brown fibers to light brown fibers.

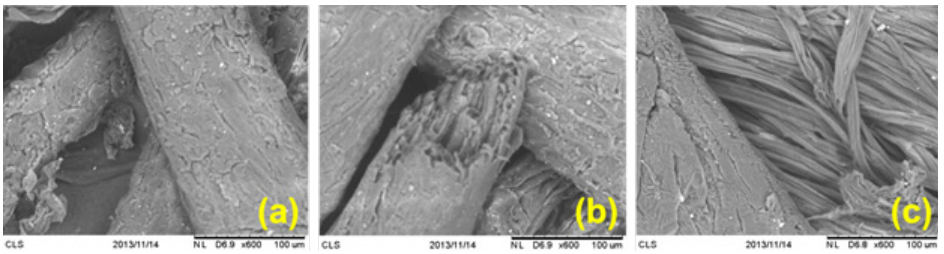

Figure 1. SEM images of (a) CLS pristine fibers, (b) after Soxhlet dewaxing and (c) direct alkaline delignification treatment.

The 5 % NaOH alkaline treatment, without dewaxing, was done to not only remove the extractives present in the sample, but to also remove lignin and hemicellulose found on the surface of the fibers [44]. This step is generally unreactive to cellulose. The alkaline treatment showed a notable visual result at the instant the 5% NaOH (1:100; fiber: liquor ratio) was added. The colorless alkaline solution turned dark brown and foamy, an indication of saponification of fats present, and subsequent delignification at or of the fiber surface. After alkaline treatment, the residue had a lighter shade than the raw plant sample and Soxhlet treated fibers.

SEM analysis of the CLS pristine fibers before and after dewaxing (M1), and direct delignification step (M2) showed that the pristine CLS fibers had a rough twisted surface (Fig. 1 a). After Soxhlet extraction, the surface smoothed out (Fig. 1 b). However, the more invasive alkaline treatment was able to cause significant separation of lignocellulosic fibers (Fig. 1 c).

The bleaching step removes lignins further by attacking its ethylenic and carbonyl groups and solubilizes hemicelluloses [49,50]. It also removes chromophoric groups of lignin through oxidation. The last step, purification, removes remaining hemicelluloses, lignins, and other impurities using diluted acetic acid [41]. The extracted cellulose was light beige in color with a 23.6 - 48.7% yield.

FTIR analysis (Fig. 2) confirmed the presence of cellulose in CLS raw and in the extracted sample based on following distinctive bands: O–H stretch of cellulose appears at 3382.67 $cm^{-1,}$ and the peak at 2897.62 cm^{-1} corresponds to C-H stretching. Bands at 1161.89 cm^{-1}, 1110.88 cm^{-1} and 1047.43 cm^{-1} correspond to C-O-C and C-H stretching of the pyranose rings [43,44,51,52]. However, presence of a band at 1750 cm^{-1} indicates presence of acetyl and ester groups of hemicellulose and/or the carboxylic acid groups in the ferulic and *p*-coumeric components of lignin in CLS raw [45]. The decreased intensity of the 1750 cm^{-1} band in M1 and M2 cellulose indicates moderate success in removal of hemicellulose and lignin. The same peaks were observed for RS and RS cellulose.

The thermogravimetric analysis curves of the CLS raw fiber, M1, M2, and STD cellulose are shown in Fig. 3. All the resulting TGA curves showed a significant weight loss from 30 °C to 100 °C mainly due to evolution of adsorbed moisture. A plateau was obtained at temperatures 100 °C to 250 °C indicating thermal stability at this given range. However, at temperatures greater than 250 °C each sample gave varying response.

The CLS raw fibers showed two-step decomposition while both the M1 and M2 cellulose gave one-step disintegration. The two-step decomposition from 270 °C to 350 °C in CLS raw can be attributed to the decomposition of cellulosic materials, hemicellulose, cellulose, and pectin; the second decomposition step at 350 °C to 400 °C involves the degradation of non-cellulosic lignin [42]. The absence of the observed two-step decomposition in M1 and M2 indicates significant removal of hemicellulose and lignin from the lignocellulosic matrix [53]. RS raw and RS cellulose also had exhibited similar TGA profiles with CLS.

TGA analysis enables the detection of the onset temperature where a given material starts to disintegrate. The onset temperatures were calculated using Perkin Elmer's Pyris data analysis software and are shown in Table 3.

Table 3. Onset decomposition temperatures of cellulose samples.

Sample	Decomposition Temperature (°C)
STD cellulose	335
CLS raw	273
M1 cellulose	331
M2 cellulose	312
RS raw	264
T1 cellulose	310
T3 cellulose	324

The results indicated that the most thermally stable material was that of the cellulose standard due to a higher onset decomposition temperature obtained because of the absence of amorphous regions, hence high crystallinity and purity [42,53]. The closer the sample's decomposition temperature to the standard, the higher it's the purity and crystallinity.

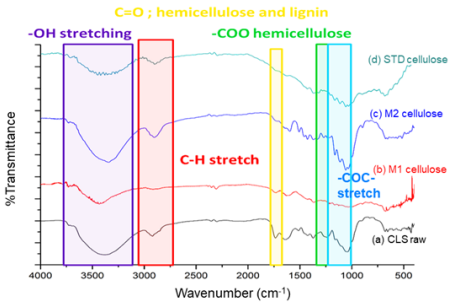

Figure 2. FT-IR spectra of (a) CLS raw, (b) M1 cellulose, (c) M2 cellulose (blue) and STD cellulose.

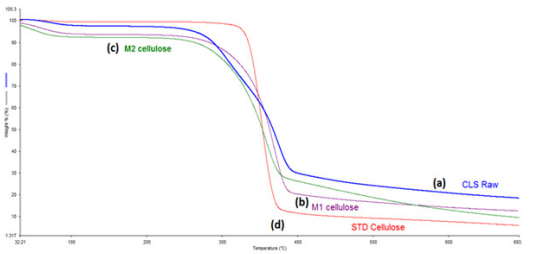

Figure 3. Thermogravimetric curves of (a) Coconut Leaf Sheath (CLS) raw, (b) M1 cellulose, (c) M2 cellulose and (d) Standard (STD) cellulose.

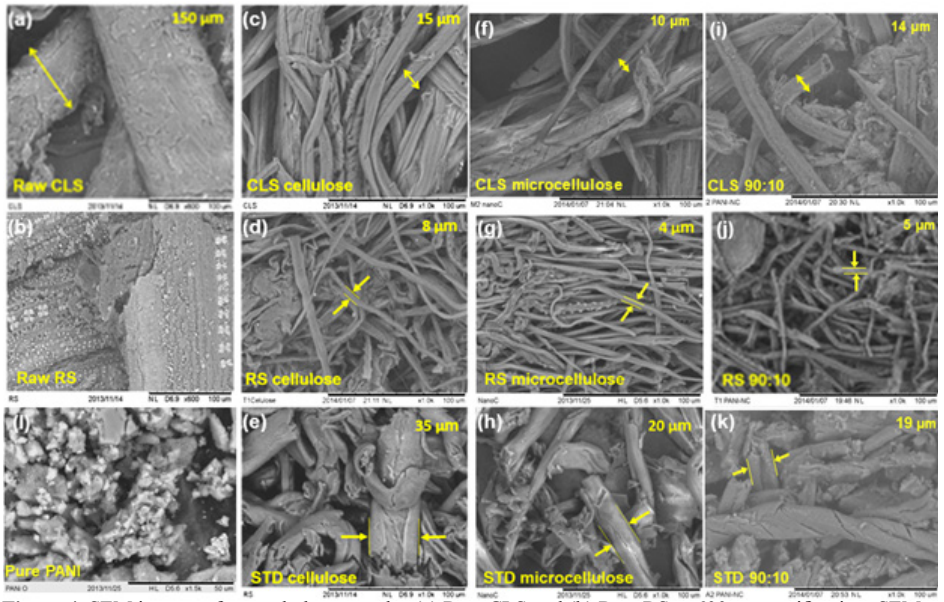

Figure 4. SEM images of ground plant samples (a) Raw CLS and (b) Raw RS at 600 x magnification; SEM images at 1000x magnification of extracted (c) CLS cellulose, (d) RS cellulose, and (e) STD cellulose; (f) CLS microcellulose, (g) RS microcellulose, and (h) STD microcellulose; PANI/MC composites (i) CLS 90:10 (ANI:MC), (j) RS 90:10 (ANI:MC), and (k) STD 90:10 (ANI:MC); and (l) pure PANI powder. Fiber diameters are indicated in the upper right-hand corner of the SEM image, except for Raw RS as no distinct fibers were observed.

Microcellulose production. To obtain MC, extracted and standard celluloses were hydrolyzed using 64% H_2SO_4 at 17.5 mL/g liquor-to-fiber ratio. Acid hydrolysis cleaves the cellulose polymer at amorphous sites obtaining MC with high crystallinity. SEM images in Fig. 4 show the reduction of fiber diameter from raw plant samples, extracted cellulose and MC. A 4 µm to 15 µm diameter decrease after acid hydrolysis was observed.

After acid hydrolysis, the SEM micrographs showed that diameters of RS-T1 and CLS-M2 MC were more uniform compared to the other samples. The fibrils were also better dispersed and thus, these were further characterized and used to make PANI composites.

PANI/microcellulose composites. The obtained PANI/MC composites formed a thick green film upon drying after vacuum filtration. Based on a visual inspection of the material, a more uniform and smoother film was observed as the amount of ANI used during the polymerization increased. However, based on visual inspection when clusters of MC fibers were not thoroughly dispersed after sonication, these fibers appear embedded into the composite surface after polymerization, producing an uneven surface.

Surface morphology. PANI composites were synthesized under constant stirring at 200 rpm, to obtain a uniform coating on the MC fibers. SEM images showed that more uniform sized PANI particles were produced with stirring compared to without stirring.

SEM images show that raw CLS and RS (Fig. 4 a – b) have rough surfaces. The morphology then changes after extraction, as cellulose (Fig. 4 c – e) appears as smooth ribbon-like fibers. The extracted cellulose fibers then decrease in diameter after acid treatment to produce MC (Fig. 4 f – h). Polymerizing PANI onto MC (Fig. 4 i - k) causes MC fibers to become rough due to the presence of PANI, which forms globular structures on the surface, similar to the morphology of pure PANI in Fig. 4 l.

Conductivity. Conductivity (σ) is a valuable characteristic of an electrode material. Electrode materials should have high conductivity for the quick movement of charge within the material. The conductivity of the PANI/MC composites were measured using the four-point probe technique. Figure 5 shows that composite conductivity values increase with the amount of ANI monomer added during polymerization as the 90:10 PANI:MC composites exhibited the highest conductivity values (36.4 μS cm^{-1} – 39.0 μS cm^{-1}). The ANI amount used corresponds to the PANI content of the composite. PANI has a theoretical conductivity of 10^{-10} to 10^{2} S cm^{-1}, while MC is an insulator, thus increasing PANI content leads to increased conductivity [54]. The 90:10 composites where then further characterized by FTIR and TGA.

FTIR analysis. FTIR spectra of the PANI/MC composites, including PANI and cellulose are shown in Fig. 6. The distinctive broad band from O–H groups of cellulose appears at 3382.67 cm^{-1}; the peak at 2897.62 cm^{-1} corresponds to C-H stretching. Peaks at 1161.89 cm^{-1}, 1110.88 cm^{-1} and 1047.43 cm^{-1} correspond to C-O-C and C-H stretching of the pyranose rings [51,52].

Peaks of PANI at 803.24 cm^{-1} correspond to bending vibrations of C–H from p-disubstituted benzene ring, while those that around 1484.61 cm^{-1} and 1565.84 cm^{-1} are from the stretching vibration of benzenoid and quinoid moieties in the PANI chains. Peaks at 1129.58 cm^{-1} and 1290.1 cm^{-1} refer to the vibration of C–H in benzene ring and stretching of C–N bond [52]. The PANI/MC spectrum has the characteristic absorptions of both cellulose and PANI that are present in the FTIR spectrum of the composite.

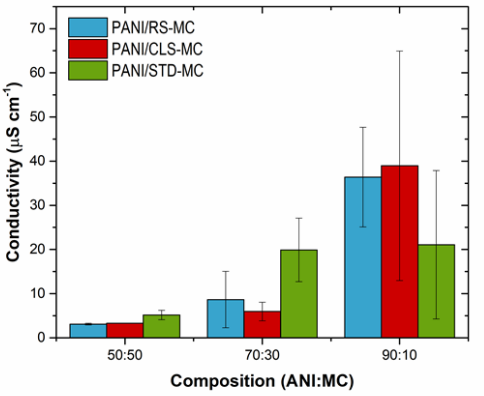

Figure 5. Conductivity values of PANI/MC composites with various ANI:MC content (n = 3, except for 50:50 PANI/CLS-MC (n = 1) as the film formed was too brittle for three measurements)

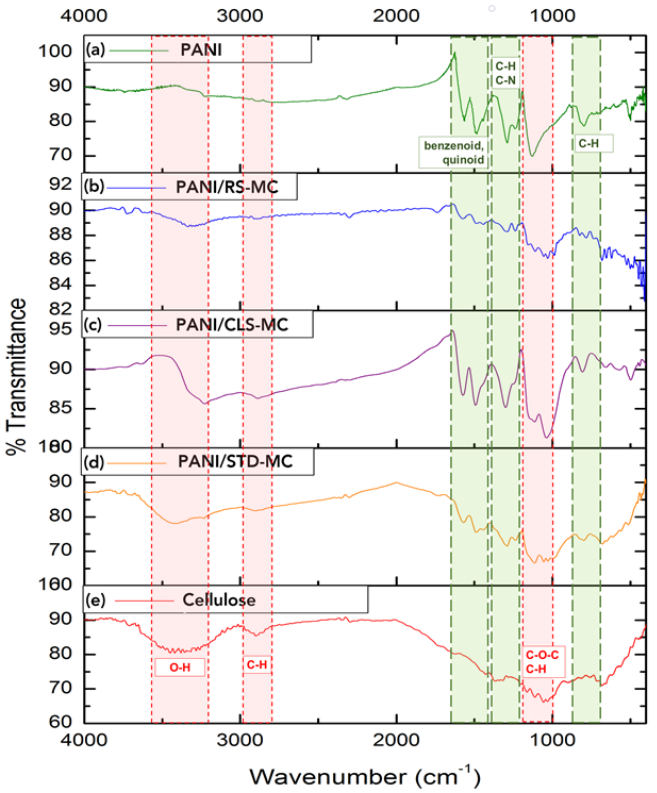

Figure 6. FTIR spectra of (a) PANI; (b) PANI/RS-MC (90:10), (c) PANI/CLS-MC (90:10), (d) PANI/STD-MC (90:10), and (e) cellulose.

The analysis of the FTIR spectra shows that the PANI/MC composites have less prominent IR bands as compared to their individual components, PANI and cellulose alone. PANI/RS-MC, in particular, has less prominent benzenoid and quinoid ring stretching vibrations and C-N bond stretching vibrations as compared to PANI/CLS-MC and PANI/STD-MC. This decrease in peak intensity can be attributed to the strong interfacial interaction of PANI and RS-MC [55–57].

Thermal stability. The TG curves of PANI/MC 90:10 composite (Fig. 7) indicates that weight loss occurred in three steps. A reduction of sample weight observed within 100 °C is due to the evolution of moisture. Second, in the region 200 °C to 300 °C; this weight loss is due to the disintegration of cellulose in composite. The final step is observed from 375 °C to 700 °C, attributed to the thermal-oxidative degradation of PANI. It can also be noted that in the region 350°C to 700 °C, there is a smaller weight % loss in the composites than the pure cellulose. It is because of the PANI that was synthesized on the cellulose's surface, providing protection from thermo-oxidative degradation. Hence, the thermal stability of cellulose is markedly increased by incorporation of PANI. This behavior is consistent with the result obtained by Mo and co-workers [52].

Cyclic voltammetry. Cyclic voltammetry was used to analyze the electrochemical properties and calculate the specific capacitance (C_m) of the composites. Specific capacitance is an important parameter of supercapacitor electrode materials, as it is the measure of charge that can be stored per gram of material. The higher the specific capacitance, the better the performance of the electrode material. Pseudocapacitive materials exhibit higher specific capacitance values than carbon materials due to the redox reactions involved.

The cyclic voltammograms (Fig. 8 a) of the PANI/MC composites and PANI show the redox reactions of PANI. The peaks A1/C1 are due to the leucoemeraldine to emeraldine redox transition, while A2/C2 are attributed to the benzenoid to quinoid reaction, both reactions are independent of pH values and tend to occur quickly [46,58–60]. The third peaks A3/C3 is caused by the oxidation of emeraldine to pernigraniline. A3 produces a very broad oxidation peak compared to A1, which indicates that this reaction has poorer charge transfer [61]. The emeraldine to pernigraniline transition involves the deprotonation of PANI and is affected by pH of the electrolyte, 1 M H_2SO_4, as the reaction occurs at a slower pace in acidic environments [60,62].

The cyclic voltammograms in Fig. 8 a are quasi-rectangular in shape with less pronounced current waves or redox peaks, indicating the dominant surface pseudocapative nature of the PANI [63,64]. Surface pseudocapacitance quickly stores electrical energy via electric double layer capacitance and fast and reversible redox processes at the surface of the electrode [63,65,66]. The specific capacitance, amount of charge stored by the material, is based on the area under the CV curve. This area increases with the addition of MC to PANI leading to better specific capacitance values. This also shows while MC increases the capacitance of the composite, it does not inhibit the Faradaic processes of PANI.

The specific capacitance values of the PANI/MC composites with increasing ANI:MC ratios, are compared with PANI in Fig. 8 b. The PANI/MC composites with higher PANI content produced higher specific capacitance values, due to the pseudocapacitive properties of PANI. The calculated specific capacitance of PANI/RS-MC (90:10) was 94.7 F g^{-1} while for PANI/CLS-MC the value was 109 F g^{-1}. PANI/MC (90:10) composites, however, exhibited noticeable higher specific capacitance than PANI (38.0 F g^{-1}) alone, indicating improvement of capacitive properties with the presence of a small amount of MC. MC is non-electroactive and an insulator, but MC aids capacitance values because of intertwined, thin ribbon-like structure, which provides a large surface area for the adhesion of PANI. The improved specific capacitance values of the PANI/MC composites compared to PANI alone can be attributed to the good adhesion of PANI onto the thin strands of MC, as seen in the SEM images (Fig. 4) and FTIR spectra (Fig. 6). Coating PANI onto MC led to higher surface areas due to the 3D structure of the MC fibers, promoted better ion diffusion and accelerated electron transport due to shorter charge transport paths within the electrode material, and improved the accessibility of electrochemical-active sites producing higher specific capacitance values compared to PANI alone [24,58,64].

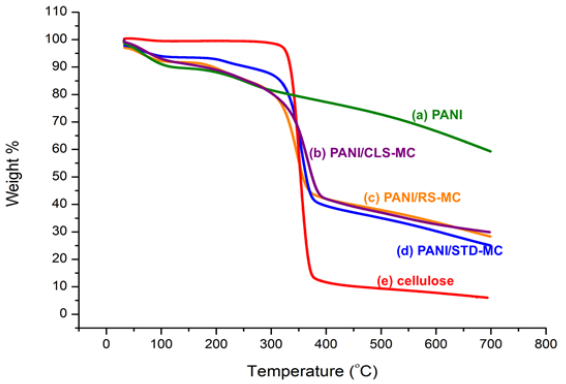

Figure 7. TGA profiles of (a) PANI, (b) PANI/CLS-MC (90:10), (c) PANI/RS-MC (90:10), (d) PANI/STD-MC (90:10) composites, and (e) cellulose.

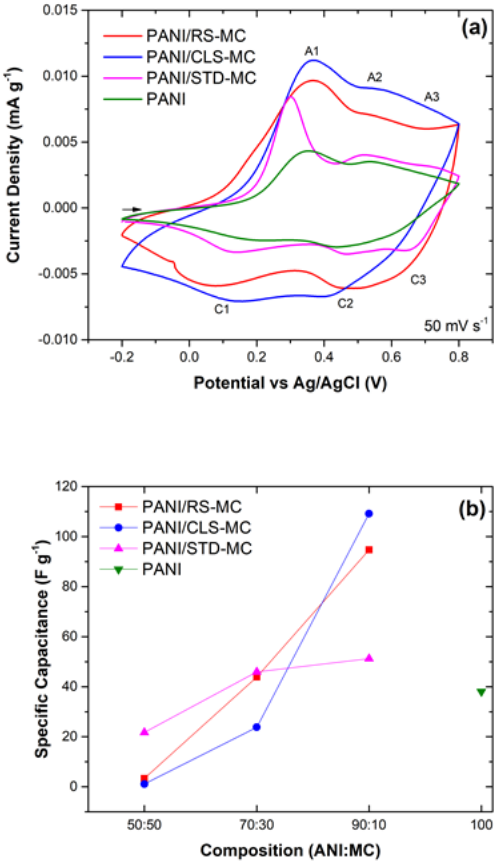

Figure 8. (a) Cyclic voltammograms of the 90:10 PANI/MC composites and PANI measured at a scan rate of 50 mV s^{-1} in 1 M H_2SO_4 (10^{th} cycle), and (b) specific capacitance values of PANI, and PANI/MC composites with various ANI:MC content measured at 50 mV s^{-1}.

Conclusion

Cellulose was successfully extracted from coconut leaf sheaths and rice stalks using delignification and bleaching methods giving 45 % and 28 % yield, respectively. SEM images showed a 5 μm decrease in diameter when the extracted cellulose was acid hydrolyzed to MC. PANI/MC composites showed a smooth to rough surface transition indicating effective PANI coating. FTIR spectra of the composites showed less prominent characteristic peaks of both pure PANI and MC, indicating good adhesion of PANI. TGA analysis showed composites are thermally stable, with profiles similar to cellulose and PANI. As supercapacitor electrode materials, the 90:10 composites exhibited the highest conductivity values of 36 μScm^{-1} to 39.0 μScm^{-1} and PANI/RS-MC and PANI/CLS-MC produced better specific capacitance values with 94.7 F g^{-1} to 109 F g^{-1} at 50 mV s^{-1}, respectively, compared to pure PANI (38.0 F g^{-1}) and PANI/STD-MC. The thin strands of RS-MC and CLS-MC improved the ion diffusion and electron transport within the electrode. The results showed that PANI/MC composites are promising supercapacitor electrode materials, and this is an effective utilization of waste residues.

Acknowledgment

This work was funded by the University of Santo Tomas – Research Center for the Natural and Applied Sciences (UST-RCNAS).

Conflict of Interest

The authors declare no conflict of interest.

Author Contributions

Conceptualization, ASKP, RDG, FCRP, and CAB; methodology, ASKP, RDG, and FCRP; data collection ASKP and RDG.; analysis and interpretation of data, ASKP, RDG, FCRP; original draft preparation, FCRP, ASKP, RDG; review and editing of the draft, CAB.

All authors have read and agreed to the final version of the manuscript.

Institutional Review Board Statement

Not applicable.

Informed Consent Statement

Not applicable.

References

[1] G.P. Wang, L. Zhang, J.J. Zhang, A review of electrode materials for electrochemical supercapacitors, Chem. Soc. Rev. 41 (2012) 797–828. https://doi.org/Doi 10.1039/C1cs15060j.

[2] P. Simon, Y. Gogotsi, Charge storage mechanism in nanoporous carbons and its consequence for electrical double layer capacitors, Philos. Trans. R. Soc. A Math. Phys. Eng. Sci. 368 (2010) 3457–3467. https://doi.org/DOI 10.1098/rsta.2010.0109.

[3] F. Bourdet, J.; Hait, J.F.; Demarthon, Energy the storage challenge, CNRS Int. Mag. (2013) 18–19. www.cnrs.fr/fr/pdf/cim/CIM30.pdf.

[4] J.M. Baptista, J.S. Sagu, U.W. KG, K. Lobato, State-of-the-art materials for high power and high energy supercapacitors: Performance metrics and obstacles for the transition from lab to industrial scale – A critical approach, Chem. Eng. J. 374 (2019) 1153–1179. https://doi.org/10.1016/j.cej.2019.05.207.

[5] M.M. Rahman, P.M. Joy, M.N. Uddin, M.Z. Bin Mukhlish, M.M.R. Khan, Improvement of Capacitive Performance of Polyaniline based Hybrid Supercapacitor, Heliyon. 7 (2021) e07407. https://doi.org/10.1016/j.heliyon.2021.e07407.

[6] Miret. S., Storage Wars: Batteries vs Supercapacitors, Berkeley Energy Resour. Collab. (2013). http://berc.berkeley.edu/storage-wars-batteries-vs-supercapacitors/ (accessed May 1, 2017).

[7] P. Yilmaz Erdogan, H. Zengin, A. Yavuz, Growth and cycling of polyaniline electrode in a deep eutectic solvent: A new electrolyte for supercapacitor applications, Solid State Ionics. 352 (2020) 115362. https://doi.org/10.1016/j.ssi.2020.115362.

[8] X. Xiao, T. Li, P. Yang, Y. Gao, H. Jin, W. Ni, W. Zhan, X. Zhang, Y. Cao, J. Zhong, L. Gong, W.C. Yen, W. Mai, J. Chen, K. Huo, Y.L. Chueh, Z.L. Wang, J. Zhou, Fiber-based all-solid-state flexible supercapacitors for self-powered systems, ACS Nano. 6 (2012) 9200–9206. https://doi.org/10.1021/nn303530k.

[9] P. Simon, Y. Gogotsi, Materials for electrochemical capacitors, Nat. Mater. (2011) 3–5. https://doi.org/10.1038/nmat2297.

[10] Z. Chang, X. An, X. Qian, High mass loading polyaniline layer anchored cellulose fibers: Enhanced interface junction for high conductivity and flame retardancy, Carbohydr. Polym. 230 (2020) 115660. https://doi.org/10.1016/j.carbpol.2019.115660.

[11] X. Chen, P. Liu, C. Liu, G. Liu, J. Wei, J. Xu, Q. Jiang, X. Liu, F. Jiang, Microstructure control for high-capacitance polyaniline, Electrochim. Acta. (2021) 138977. https://doi.org/10.1016/j.electacta.2021.138977.

[12] G.A. Snook, P. Kao, A.S. Best, Conducting-polymer-based supercapacitor devices and electrodes, J. Power Sources. 196 (2011) 1–12. https://doi.org/10.1016/j.jpowsour.2010.06.084.

[13] Y. Zhou, Z. Qin, L. Li, Y. Zhang, Y. Wei, L. Wang, M. Zhu, Electrochimica Acta Polyaniline / multi-walled carbon nanotube composites with core – shell structures as supercapacitor electrode materials, Electrochim. Acta. 55 (2010) 3904–3908. https://doi.org/10.1016/j.electacta.2010.02.022.

[14] M.H. Salehi, H. Golbaten-Mofrad, S.H. Jafari, V. Goodarzi, M. Entezari, M. Hashemi, S. Zamanlui, Electrically conductive biocompatible composite aerogel based on nanofibrillated template of bacterial cellulose/polyaniline/nano-clay, Int. J. Biol. Macromol. 173 (2021) 467–480. https://doi.org/10.1016/j.ijbiomac.2021.01.121.

[15] Q. Li, J. Liu, J. Zou, A. Chunder, Y. Chen, L. Zhai, Synthesis and electrochemical performance of multi-walled carbon nanotube/polyaniline/MnO2 ternary coaxial nanostructures for supercapacitors, J. Power Sources. 196 (2011) 565–572. https://doi.org/10.1016/j.jpowsour.2010.06.073.

[16] Q. Liu, M.H. Nayfeh, S.T. Yau, Brushed-on flexible supercapacitor sheets using a nanocomposite of polyaniline and carbon nanotubes, J. Power Sources. 195 (2010) 7480–7483. https://doi.org/10.1016/j.jpowsour.2010.06.002.

[17] V. Gupta, N. Miura, Polyaniline/single-wall carbon nanotube (PANI/SWCNT) composites for high performance supercapacitors, Electrochim. Acta. 52 (2006) 1721–1726. https://doi.org/10.1016/j.electacta.2006.01.074.

[18] R. Awata, M. Shehab, A. El Tahan, M. Soliman, S. Ebrahim, High performance supercapacitor based on camphor sulfonic acid doped polyaniline/multiwall carbon nanotubes nanocomposite, Electrochim. Acta. 347 (2020) 136229. https://doi.org/10.1016/j.electacta.2020.136229.

[19] K.S. Lee, C.W. Park, I. Phiri, J.M. Ko, New design for Polyaniline@Multiwalled carbon nanotubes composites with bacteria doping for supercapacitor electrodes, Polymer (Guildf). 210 (2020) 123014. https://doi.org/10.1016/j.polymer.2020.123014.

[20] Y.N. Liu, L.N. Jin, H.T. Wang, X.H. Kang, S.W. Bian, Fabrication of three-dimensional composite textile electrodes by metal-organic framework, zinc oxide, graphene and polyaniline for all-solid-state supercapacitors, J. Colloid Interface Sci. 530 (2018) 29–36. https://doi.org/10.1016/j.jcis.2018.06.062.

[21] H. Wang, E. Zhu, J. Yang, P. Zhou, D. Sun, W. Tang, Bacterial cellulose nanofiber-supported polyaniline nanocomposites with flake-shaped morphology as supercapacitor electrodes, J. Phys. Chem. C. 116 (2012) 13013–13019. https://doi.org/10.1021/jp301099r.

[22] U.M. Casado, R.M. Quintanilla, M.I. Aranguren, N.E. Marcovich, Composite films based on shape memory polyurethanes and nanostructured polyaniline or cellulose-polyaniline particles, Synth. Met. 162 (2012) 1654–1664. https://doi.org/10.1016/j.synthmet.2012.07.020.

[23] Z. Shi, S. Zang, F. Jiang, L. Huang, D. Lu, Y. Ma, G. Yang, In situ nano-assembly of bacterial cellulose–polyaniline composites, RSC Adv. 2 (2012) 1040. https://doi.org/10.1039/c1ra00719j.

[24] Y. Li, Q. Gong, X. Liu, Z. Xia, Y. Yang, C. Chen, C. Qian, Wide temperature-tolerant polyaniline/cellulose/polyacrylamide hydrogels for high-performance supercapacitors and motion sensors, Carbohydr. Polym. 267 (2021) 118207. https://doi.org/10.1016/j.carbpol.2021.118207.

[25] X. Zhang, Z. Lin, B. Chen, W. Zhang, S. Sharma, W. Gu, Y. Deng, Solid-state flexible polyaniline/silver cellulose nanofibrils aerogel supercapacitors, J. Power Sources. 246 (2014) 283–289. https://doi.org/10.1016/j.jpowsour.2013.07.080.

[26] N.R. Aswathy, S.A. Kumar, S. Mohanty, S.K. Nayak, A.K. Palai, Polyaniline/multi-walled carbon nanotubes filled biopolymer based flexible substrate electrodes for supercapacitor applications, J. Energy Storage. 35 (2021) 102256. https://doi.org/10.1016/j.est.2021.102256.

[27] C. Yang, D. Li, Flexible and foldable supercapacitor electrodes from the porous 3D network of cellulose nanofibers, carbon nanotubes and polyaniline, Mater. Lett. 155 (2015) 78–81. https://doi.org/10.1016/j.matlet.2015.04.096.

[28] K. Wang, P. Zhao, X. Zhou, H. Wu, Z. Wei, Flexible supercapacitors based on cloth-supported electrodes of conducting polymer nanowire array/SWCNT composites, J. Mater. Chem. 21 (2011) 16373. https://doi.org/10.1039/c1jm13722k.

[29] J. Wen, B. Xu, Y. Gao, M. Li, H. Fu, Wearable technologies enable high-performance textile supercapacitors with flexible, breathable and wearable characteristics for future energy storage, Energy Storage Mater. 37 (2021) 94–122. https://doi.org/10.1016/j.ensm.2021.02.002.

[30] P. Song, X. He, M. Xie, J. Tao, X. Shen, Z. Ji, Z. Yan, L. Zhai, A. Yuan, Polyaniline wrapped graphene functionalized textile with ultrahigh areal capacitance and energy density for high-performance all-solid-state supercapacitors for wearable electronics, Compos. Sci. Technol. 198 (2020) 108305. https://doi.org/10.1016/j.compscitech.2020.108305.

[31] L.N. Jin, F. Shao, C. Jin, J.N. Zhang, P. Liu, M.X. Guo, S.W. Bian, High-performance textile supercapacitor electrode materials enhanced with three-dimensional carbon nanotubes/graphene conductive network and in situ polymerized polyaniline, Electrochim. Acta. 249 (2017) 387–394. https://doi.org/10.1016/j.electacta.2017.08.035.

[32] K.G. Satyanarayana, G.G.C. Arizaga, F. Wypych, Biodegradable composites based on lignocellulosic fibers-An overview, Prog. Polym. Sci. 34 (2009) 982–1021. https://doi.org/10.1016/j.progpolymsci.2008.12.002.

[33] S.J. Eichhorn, Cellulose nanowhiskers: promising materials for advanced applications, Soft Matter. 7 (2011) 303. https://doi.org/10.1039/c0sm00142b.

[34] J. Biagiotti, D. Puglia, J.M. Kenny, A Review on Natural Fibre-Based Composites-Part I, J. Nat. Fibers. 1 (2004) 37–68. http://www.tandfonline.com/doi/abs/10.1300/J395v01n02_04.

[35] R.J. Moon, A. Martini, J. Nairn, J. Simonsen, J. Youngblood, Cellulose nanomaterials review: structure, properties and nanocomposites, 2011. https://doi.org/10.1039/c0cs00108b.

[36] World Bank, Agricultural land - Philippines, World Bank Open Data. (2018). https://data.worldbank.org/indicator/AG.LND.AGRI.ZS?locations=PH (accessed July 30, 2021).

[37] A.S. Chiu, J.Z. Sengson, Philippine Biomass Utilization: A country paper report, (2004). http://www.aist-riss.jp/old/lca/ci/activity/project/biomass/report/041028_paper/chiu_paper.pdf.

[38] FAO, Women in Agriculture, Environment and Rural Production, Fact Sheet Philipp. (n.d.). http://www.fao.org/3/ae946e/ae946e03.htm (accessed July 30, 2021).

[39] Department of Agriculture - Philippine Rice Research Institute, Don't burn rice straw, (2016). https://www.philrice.gov.ph/dont-burn-rice-straw-philrice/ (accessed July 30, 2021).

[40] L. Huang, S. Wang, Y. Zhang, X.H. Huang, J.J. Peng, F. Yang, Preparation of a N-P co-doped waste cotton fabric-based activated carbon for supercapacitor electrodes, Xinxing Tan Cailiao/New Carbon Mater. 36 (2021) 1128–1137. https://doi.org/10.1016/S1872-5805(21)60054-9.

[41] S.M.L. Rosa, N. Rehman, M.I.G. De Miranda, S.M.B. Nachtigall, C.I.D. Bica, Chlorine-free extraction of cellulose from rice husk and whisker isolation, Carbohydr. Polym. 87 (2012) 1131–1138. https://doi.org/10.1016/j.carbpol.2011.08.084.

[42] M.A. Islam, H.L. Ong, A.R. Villagracia, K.A. Khairul, A.B. Ganganboina, R.A. Doong, Biomass–derived cellulose nanofibrils membrane from rice straw as sustainable separator for high performance supercapacitor, Ind. Crops Prod. 170 (2021) 113694. https://doi.org/10.1016/j.indcrop.2021.113694.

[43] T. Gabriel, A. Belete, F. Syrowatka, R.H.H. Neubert, T. Gebre-Mariam, Extraction and characterization of celluloses from various plant byproducts, Int. J. Biol. Macromol. 158 (2020) 1248–1258. https://doi.org/10.1016/j.ijbiomac.2020.04.264.

[44] G. Akhlamadi, E.K. Goharshadi, S.V. Saghir, Extraction of cellulose nanocrystals and fabrication of high alumina refractory bricks using pencil chips as a waste biomass source, Ceram. Int. (2021). https://doi.org/10.1016/j.ceramint.2021.06.117.

[45] N. Johar, I. Ahmad, A. Dufresne, Extraction, preparation and characterization of cellulose fibres and nanocrystals from rice husk, Ind. Crops Prod. 37 (2012) 93–99. https://doi.org/10.1016/j.indcrop.2011.12.016.

[46] S.M. Suresh Kumar, D. Duraibabu, K. Subramanian, Studies on mechanical, thermal and dynamic mechanical properties of untreated (raw) and treated coconut sheath fiber reinforced epoxy composites, Mater. Des. 59 (2014) 63–69. https://doi.org/10.1016/j.matdes.2014.02.013.

[47] N. Syaftika, Y. Matsumura, Comparative study of hydrothermal pretreatment for rice straw and its corresponding mixture of cellulose, xylan, and lignin, Bioresour. Technol. 255 (2018) 1–6. https://doi.org/10.1016/j.biortech.2018.01.085.

[48] H. Kargarzadeh, M. Ioelovich, I. Ahmad, S. Thomas, A. Dufresne, Methods for Extraction of Nanocellulose from Various Sources, Handb. Nanocellulose Cellul. Nanocomposites. (2017) 1–49. https://doi.org/10.1002/9783527689972.ch1.

[49] G.X. Pan, J.L. Bolton, G.J. Leary, Determination of Ferulic and p-Coumaric Acids in Wheat Straw and the Amounts Released by Mild Acid and Alkaline Peroxide Treatment, J. Agric. Food Chem. 46 (1998) 5283–5288. https://doi.org/10.1021/jf980608f.

[50] M.A. Hubbe, O.J. Rojas, L.A. Lucia, M. Sain, Cellulosic nanocomposites: A review, Int. J. Interact. Mob. Technol. 12 (2018) 929–980. https://doi.org/10.15376/biores.3.3.929-980.

[51] C. Uma Maheswari, K. Obi Reddy, E. Muzenda, B.R. Guduri, A. Varada Rajulu, Extraction and characterization of cellulose microfibrils from agricultural residue - Cocos nucifera L, Biomass and Bioenergy. 46 (2012) 555–563. https://doi.org/10.1016/j.biombioe.2012.06.039.

[52] Z. li Mo, Z. li Zhao, H. Chen, G. ping Niu, H. feng Shi, Heterogeneous preparation of cellulose-polyaniline conductive composites with cellulose activated by acids and its electrical properties, Carbohydr. Polym. 75 (2009) 660–664. https://doi.org/10.1016/j.carbpol.2008.09.010.

[53] Q. Lin, Y. Huang, W. Yu, Effects of extraction methods on morphology, structure and properties of bamboo cellulose, Ind. Crops Prod. 169 (2021) 113640. https://doi.org/10.1016/j.indcrop.2021.113640.

[54] J. Stejskal, M. Trchová, P. Bober, P. Humpolíček, V. Kašpárková, I. Sapurina, M.A. Shishov, M. Varga, Conducting Polymers: Polyaniline, 2015. https://doi.org/10.1002/0471440264.pst640.

[55] A.R. Pai, T. Binumol, D.A. Gopakumar, D. Pasquini, B. Seantier, N. Kalarikkal, S. Thomas, Ultra-fast heat dissipating aerogels derived from polyaniline anchored cellulose nanofibers as sustainable microwave absorbers, Carbohydr. Polym. 246 (2020) 116663. https://doi.org/10.1016/j.carbpol.2020.116663.

[56] Y. Wan, J. Li, Z. Yang, H. Ao, L. Xiong, H. Luo, Simultaneously depositing polyaniline onto bacterial cellulose nanofibers and graphene nanosheets toward electrically conductive nanocomposites, Curr. Appl. Phys. 18 (2018) 933–940. https://doi.org/10.1016/j.cap.2018.05.008.

[57] N.C. Nepomuceno, A.A.A. Seixas, E.S. Medeiros, T.J.A. Mélo, Evaluation of conductivity of nanostructured polyaniline/cellulose nanocrystals (PANI/CNC) obtained via in situ polymerization, J. Solid State Chem. 302 (2021). https://doi.org/10.1016/j.jssc.2021.122372.

[58] P. Das, S. Mondal, S. Malik, Fully organic polyaniline nanotubes as electrode material for durable supercapacitor, J. Energy Storage. 39 (2021) 102662. https://doi.org/10.1016/j.est.2021.102662.

[59] M. Yu, W. Wang, C. Li, T. Zhai, X. Lu, Y. Tong, Scalable self-growth of Ni@NiO core-shell electrode with ultrahigh capacitance and super-long cyclic stability for supercapacitors, NPG Asia Mater. 6 (2014) e129. http://dx.doi.org/10.1038/am.2014.78.

[60] E. Song, J.W. Choi, Conducting polyaniline nanowire and its applications in chemiresistive sensing, Nanomaterials. 3 (2013) 498–523. https://doi.org/10.3390/nano3030498.

[61] S. Pruneanu, E. Veress, I. Marian, L. Oniciu, Characterization of polyaniline by cyclic voltammetry and UV-Vis absorption spectroscopy, J. Mater. Sci. 34 (1999) 2733–2739. https://doi.org/10.1023/A:1004641908718.

[62] F. Huerta, C. Quijada, F. Montilla, E. Morallón, Revisiting the Redox Transitions of Polyaniline. Semiquantitative Interpretation of Electrochemically Induced IR Bands, J. Electroanal. Chem. 897 (2021) 115593. https://doi.org/10.1016/j.jelechem.2021.115593.

[63] N.R. Chodankar, H.D. Pham, A.K. Nanjundan, J.F.S. Fernando, K. Jayaramulu, D. Golberg, Y.K. Han, D.P. Dubal, True Meaning of Pseudocapacitors and Their Performance Metrics: Asymmetric versus Hybrid Supercapacitors, Small. 16 (2020) 1–35. https://doi.org/10.1002/smll.202002806.

[64] T. Schoetz, L.W. Gordon, S. Ivanov, A. Bund, D. Mandler, R.J. Messinger, Disentangling faradaic, pseudocapacitive, and capacitive charge storage: A tutorial for the characterization of batteries, supercapacitors, and hybrid systems, Electrochim. Acta. 412 (2022) 140072. https://doi.org/10.1016/j.electacta.2022.140072.

[65] M. Forghani, S.W. Donne, Method Comparison for Deconvoluting Capacitive and Pseudo-Capacitive Contributions to Electrochemical Capacitor Electrode Behavior, J. Electrochem. Soc. 165 (2018) A664–A673. https://doi.org/10.1149/2.0931803jes.

[66] Y. Gogotsi, R.M. Penner, Energy Storage in Nanomaterials - Capacitive, Pseudocapacitive, or Battery-like?, ACS Nano. 12 (2018) 2081–2083. https://doi.org/10.1021/acsnano.8b01914.